

PAPER • OPEN ACCESS


# Investigation of methods to quantify silver screen-printed onto cellulosic substrate: towards recycling of printed electronics

To cite this article: João H F Conceição *et al* 2023 *Flex. Print. Electron.* **8** 035014

View the [article online](#) for updates and enhancements.

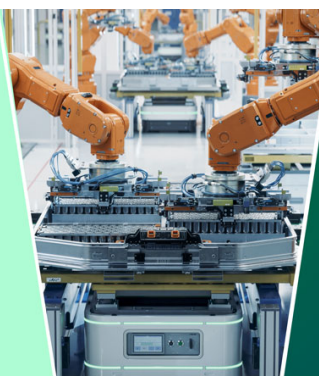
## You may also like

- [Assessing sustainability hotspots in the production of paper-based printed electronics](#)  
Akshat Sudheshwar, Valerio Beni, Nadia Malinverno *et al.*
- [Brain networks of rats under anesthesia using resting-state fMRI: comparison with dead rats, random noise and generative models of networks](#)  
G J-P C Becq, E L Barbier and S Achard
- [Development of a robust fabrication process for single silicon nanowire-based omega gate transistors on polyamide substrate](#)  
T Arjmand, M Legallais, T Haffner *et al.*




The  
Electrochemical  
Society

Advancing solid state &  
electrochemical science & technology



DISCOVER  
how sustainability  
intersects with  
electrochemistry & solid  
state science research



# Flexible and Printed Electronics



## PAPER

### OPEN ACCESS

RECEIVED  
17 January 2023

REVISED  
31 July 2023

ACCEPTED FOR PUBLICATION  
17 August 2023

PUBLISHED  
11 September 2023

Original content from  
this work may be used  
under the terms of the  
[Creative Commons  
Attribution 4.0 licence](#).

Any further distribution  
of this work must  
maintain attribution to  
the author(s) and the title  
of the work, journal  
citation and DOI.



## Investigation of methods to quantify silver screen-printed onto cellulosic substrate: towards recycling of printed electronics

João H F Conceição<sup>1,2</sup> , M Party<sup>1</sup>, D Curtil<sup>1</sup> , L Švecová<sup>2</sup> , N Marlin<sup>1</sup> and N Reverdy-Bruas<sup>1,\*</sup>

<sup>1</sup> University Grenoble Alpes, CNRS, Grenoble INP (Institute of Engineering University Grenoble Alpes), LGP2, 38000 Grenoble, France

<sup>2</sup> University Grenoble Alpes, University Savoie Mont Blanc, CNRS, Grenoble INP (Institute of Engineering University Grenoble Alpes), LEPMI, 38000 Grenoble, France

\* Author to whom any correspondence should be addressed.

E-mail: [nadege.reverdy-bruas@grenoble-inp.fr](mailto:nadege.reverdy-bruas@grenoble-inp.fr)

**Keywords:** silver, quantification, paper-based electronics, RFID antenna

### Abstract

The continued progress in electronics technology has led to unsustainable consumption of plastic-based products containing, in their majority, natural finite metallic resources. The substitution of these plastic materials by more sustainable ones, such as cellulosic substrates, is one of many measures applied by the industry to reduce their environmental impact. In this work, due to the lack of information in the literature, a fast and accurate method to measure the amount of metal deposited onto a paper-based substrate is proposed. The development of this method will contribute to the creation of a procedure for determining the quantity of metal present in end-of-life printed electronics. The present work investigates and compares four different methodologies. Image processing and geometrical analyses presented overestimated and non-precise results for printed Ag. A third method based on gravimetric measurements presented to be more accurate compared with the previous methods. The last method based on acid leaching of the printed electronic ashes outcome to be the more precise, reliable and simpler method, and overcomes challenges associated to the printed pattern geometry and the materials used during its production. These results will provide key information for the development of a quantitative methodology to determine the percentage of Ag used in paper-based electronics that can be adapted easily by the industry. Furthermore, this method is a prerequisite for recycling processes devoted to this type of electronics after reaching their end-of-life, considering Ag as one of the major components to be separated and, further, valorized.

## 1. Introduction

The continuous demand for the Internet of Things aiming to supply comfort and welfare to citizens [1–3] enhances the demand concerning the manufacturing of low-cost, lightweight, small, thin and flexible, smart, and disposable devices. Conventional electronics based on silicon material dominate the high-end electronics applications with high integration density and high switching speed in the future. However, these electronics are manufactured with a high system complexity, such as the printed circuit board (PCB), which is not suitable for multiple applications.

Printed electronics (PEs) refers to the printing of circuits, interconnects, electrical components, or devices on the surface of different media

such as plastic, paper, and textile, by various printing techniques [1]. Printing processes such as flexography, gravure, screen-printing, aerosol jet and inkjet have been investigated for printed electronic applications [1, 4, 5]. Screen-printing, as one of the most mature and versatile technology, was accounted for contributing the largest market share in 2020 [6]. Functional inks for PEs are a blend of conductive materials—organic/inorganic—vehicle and additives [1, 4, 7–9]. A major part of available conductive inks is composed of metals, and among them, silver is the most common. The vehicle, fluid phase of the ink, is composed of a mixture of oligomers and polymers (resins) in one or several solvents and diluents.

Compared to the manufacturing of traditional PCBs, PE offers many advantages, such as lower manufacturing and processing costs, and an extended

range of applications due to the possibility to produce devices that can bend, flex or even stretch [10, 11]. Nevertheless, PE will not replace silicon-based structures; most of the time, hybrid systems are built that combines printed techniques and Si-based components. Along with high-speed development of the electronic industry, the consumption of plastic-based electronic products worldwide has grown significantly, as their lifetime has become shorter over time [12]. Cellulose-rich materials, like paper, constitute a promising candidate substrate to replace plastics, due to their availability, low-price, flexible character, recyclability, bio-sourced origin, and biodegradable nature. These materials are already used in everyday applications, from packaging to healthcare. Nowadays, there have been many advances in the area of paper substrates and paper electronics for application ranging from basic electronic components to more advanced devices [13–33]. The drawbacks/advantages and also the challenges offered by the use of paper for the design of PE devices have been discussed in several reviews [4, 5].

Although offering many advantages, it is however not clear yet how the PE will be considered and treated at its end-of-life. Only few publications discussed the future that can be given to these devices instead of their usual combustion [34–36]. To reduce the consumption of raw materials, and to create a more sustainable future, an eco-design strategy must be implemented within the development of PE [37–39]. In this context, new procedures should be developed to reduce PE environmental impact, through its re-use, recovery and recycling, in agreement with European Waste Framework Directive [40]. Recycling paper-based PE includes both the separation and recovery of: (i) the cellulosic fibers, that will serve to produce recycled paper; and (ii) metal-based inks, to valorize the high added value materials, especially the metals. Tracking the metals in a quantitative way, all along the lifetime of the PE, from its manufacturing to its recycling, is of primary importance to the eco-design of PE. To the best of our knowledge, this has not yet been performed.

Therefore, the objective of the present work is to establish a well-defined and precise methodology to determine the fraction of printed patterns on a PE device, and, consequently, to quantify the amount of metal printed onto the device substrate. Four different methodologies have been investigated and compared: (i) thresholding and topographical analysis of the printed patterns; (ii) topographical and geometrical analyses; (iii) gravimetric measurements; (iv) acid leaching. The first two are usually performed to qualify different printing parameters for manufacturing optimization [41–43], while the last one is proposed in this study as a suitable simple and fast methodology to quantify precisely the metal printed onto the device substrate. The four methods have been applied on a paper-based radio frequency

identification (RFID) antenna produced in our laboratory, noted as PE lab; in order to master nearly entirely its composition. Additionally, screen printing technology using a silver-based ink has been selected to replicate an effective industrial PE.

## 2. Materials and methods

### 2.1. Materials

The conductive Silver Electron<sup>®</sup>—SE—solvent-based ink, containing micro-sized silver flakes, was purchased from VFP Ink Technologies. The supplier's information available is given in table 1 [44].

In this study, a commercially available paper has been selected as substrate. It is the Powercoat<sup>™</sup> XD80, supplied by Fedrigoni. Each side of this paper is coated to improve the printing quality. Thus, it is a filler-containing paper with a basis weight of  $86 \pm 4 \text{ g m}^{-2}$  and  $87 \pm 5 \text{ }\mu\text{m}$  thickness [45]. A qualitative analysis using microscopy, shows that the paper is composed of a mixture of hardwood and softwood bleached pulps, and that it contains calcium carbonate,  $\text{CaCO}_3$ , as main filler.

For silver quantification in ash, acid leaching has been performed with nitric acid,  $\text{HNO}_3$ , (65 wt%), obtained from Roth. Distilled water was used for solution preparation.

### 2.2. Methods

#### 2.2.1. RFID antenna manufacturing—the PE lab

Classically, a functional RFID antenna is composed of a minimum of three layers: (i) a first conductive layer; (ii) an insulation layer for the bridge; (iii) a second conductive layer to close the antenna, in which the silicon chip is positioned. In this study, only the first layer of the RFID antenna was studied, since it corresponds to the layer richest in conductive material. Consequently, the first layer has the highest metal weight fraction regarding the full device mass. The layer printing was performed at ambient conditions using screen printing.

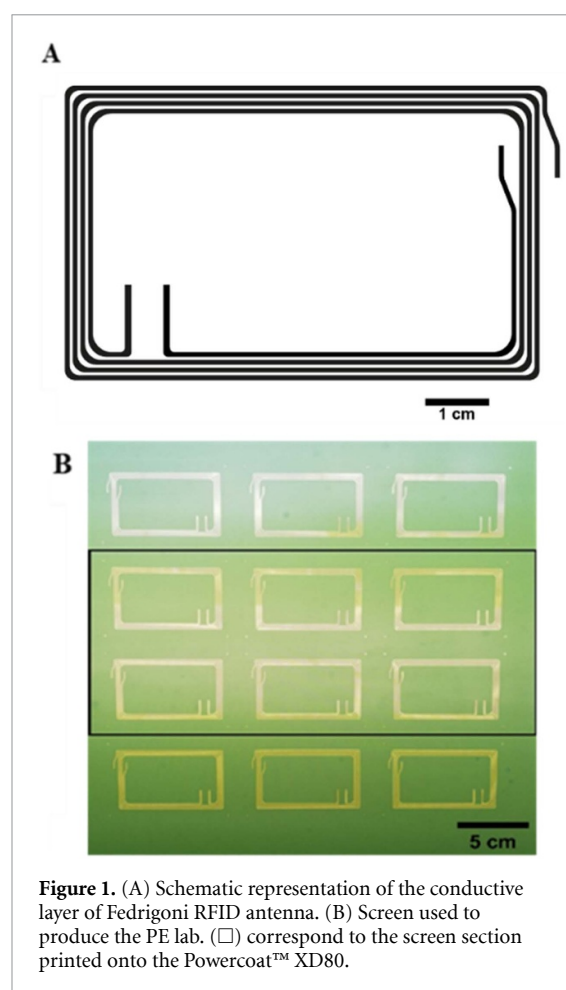
#### 2.2.2. Screen-printing

A  $7.72 \times 4.60 \text{ cm}^2$  RFID antenna pattern was supplied by Fedrigoni and printed on Powercoat<sup>™</sup> XD80 substrate. The theoretical area of the printed pattern was assessed using DWG TrueView software. The first layer, which corresponds to the conductive tracks of the RFID antenna is represented in figure 1. A screen with  $77 \text{ threads}\cdot\text{cm}^{-1}$  was used to print the first layer. Additionally, the same pattern was multiplied in order to test the reproducibility and the precision of the measurements.

The conductive tracks were printed using a semi-automatic DEK Horizon 03i screen-printer. After an optimization phase, the pressure on the squeegee was set to 11 kg. The off-contact between the screen and the substrate was set at 1 mm and a printing speed of  $150 \text{ mm s}^{-1}$ . After printing, the wet tracks were dried

**Table 1.** Properties and characterization of VFP-SE ink (taken from [44]).

Viscosity (30 rpm, 25 °C) [Pa s]		27.5
Solid content [%]		45–74
Sintering	Thermal	130 °C for 30 min 150 °C for 10 min
	NIR	2 secs
	Photonic	Few $\mu$ secs
Suitable substrates		PET; glass; polyimide; polyurethane; paper; etc.

**Figure 1.** (A) Schematic representation of the conductive layer of Fedrigoni RFID antenna. (B) Screen used to produce the PE lab. (C) correspond to the screen section printed onto the Powercoat™ XD80.

inside a Memmert UF 110 oven at 150 °C for 10 min, to promote the sintering of the metallic particles. The obtained printed material is referred as PE lab. It will be used to develop the silver quantification methods. In this study, 17 samples of each individual pattern of PE lab, a total of 102 samples, were printed and characterized.

### 2.2.3. Scanning electron microscopy-energy dispersive x-ray spectroscopy (SEM-EDS) analysis

Surface and cross-section SEM and SEM-backscattered electron (SEM-BSE) images of Powercoat™ XD80 and PE lab have been obtained

using a SEM-field emission gun JEOL JSM-IT5000HR LV, equipped with a silicon drift detector 60 mm<sup>2</sup>, supplied by Bruker. Additionally, for each image the respective SEM-EDS spectra was collected.

### 2.2.4. Thermal gravimetric analysis (TGA)

TGA thermograms were obtained using a Mettler Toledo TGA/DSC 3+ equipped with a single differential thermal analysis (SDTA) sensor, under air conditions, in the temperature range from 25 °C to 900 °C, applying a heating rate of 5 °C min<sup>-1</sup>. Different isotherms were applied at 105 °C, 525 °C, and 900 °C which correspond to the oven drying and calcination temperatures used for the other analyses. Triplicate analyses were carried out for each sample and the solid residue at 900 °C was considered a reference value corresponding to the metal quantity present in the ink, as it will be discussed in the results section.

### 2.2.5. Dry matter content determination

The dry matter content of the Powercoat™ XD80 and PE lab was performed accordingly to ISO 638:2008 [46], using 10 × 10 cm<sup>2</sup> samples. The samples were weighted before and after drying at 105 °C during 4 h minimum in an oven, using a Mettler Toledo ME204 analytic balance (precision = 0.1 mg).

### 2.2.6. Ash content determination

The quantification of ash was performed at 525 and 900 °C, accordingly to TAPPI standards T 211 om-12 [47] and T 413 om-11 [48], respectively. A Carbolite ELF 11/6B furnace was used to perform the sample calcination. The samples were shredded into small pieces and weighted before and after each heating step in order to assess the ash content evolution over the calcination. Triplicates were systematically performed to assess the ash content in the paper substrate and in the PE lab. After each calcination, the samples were stored inside a desiccator under controlled atmosphere (23.5 ± 1.0 °C and 50% ± 5% RH) before weighing [49].

### 2.2.7. Metal content determination in ash

The silver quantity in each ash was measured using a Perkin Elmer PinAAcle™ 900 T atomic absorption spectroscopy (AAS) at 328.07 nm, after prior acid digestion of the sample. The equipment was previously calibrated with six different standard solutions of silver nitrate, AgNO<sub>3</sub>, 0.1, 1, 5, 10, 50, 100 mg l<sup>-1</sup>.

The ashes obtained by calcination were added to 40 ml of an aqueous solution of nitric acid (1:3 v/v of NH<sub>3</sub>:H<sub>2</sub>O). The digestion was performed under a fume hood at 25 °C for 24 h. Then, the leached solution was centrifuged over 10 min at 7000 rpm to deposit any solid material not completely digested. Additionally, the systems were centrifuged to separate both phases. The leachate was subsequently diluted using distilled water. For the determination of the



silver concentration in each leachate, triplicates were made.

Prior to present the methodology used it is worth to mention how the results described in this work are presented. Based on multiple experimental steps, all results are presented as the mean value  $\pm$  uncertainty of the analysis, where the uncertainty corresponds to the error propagation of the different measurements.

#### 2.2.8. Quantification of deposited Ag on the substrate

Four different methodologies have been investigated to quantify Ag deposited on the PE lab: (a) thresholding and topographical analysis of the PE pattern giving the deposited ink volume, combined with the Ag density; (b) geometrical and topographical analysis of the PE pattern also giving the volume of deposited ink, combined with the Ag density; (c) gravimetric Ag determination; and finally (d) PE lab ash leaching using  $\text{HNO}_3$ . For the first two methodologies, all images of the printed tracks were obtained using an EPSON Perfection V700 Photo scanner at a resolution of 6400 pixels per inch (ppi). An Alicona InfiniteFocus IFM G4 profilometer was used in order to determine the printed line profiles. This 3D measurement allows to assess the thickness of the printed lines and surface roughness.

##### 2.2.8.1. Thresholding (image processing) and topographical analysis

Grayscale images were obtained from scanned tracks using ImageJ software. Binary images were obtained after establishing a threshold that converts pixels to white and black, depending on its intensity, as presented in equation (1),

$$\begin{cases} I_{i,j} < c \rightarrow \text{pixel} = \text{black} \\ I_{i,j} > c \rightarrow \text{pixel} = \text{white} \end{cases} \quad (1)$$

where,  $I_{i,j}$  and  $c$  correspond to image intensity and fixed constant, respectively.

Afterward, the printed area was determined by the ratio between black and white pixels. The thickness of the printed patterns was measured on different areas of the substrate, in triplicates, and an average was extracted, using the Alicona device. The printed volume was determined by multiplying the area by the thickness, as presented in the equation (2),

$$\text{Volume} = \text{printed area} \times \text{thickness}. \quad (2)$$

In order to determine an approximate value of the volume of printed metal, it was considered that after the sintering step, the patterns are mainly composed of silver and, consequently, their volume corresponds to the metal volume. A porosity factor ( $\emptyset_p$ ) of 57% was adopted based on the work of Thénod *et al.* who proposed a methodology to estimate the printed ink porosity of screen-printed patterns using micro and nano Ag-based inks [50]. This factor is necessary

for the estimation of the cost of commercial ink corresponding to a thickness of dried ink. The porosity depends on the nature of the ink particles, their concentrations, shapes and sintering conditions applied. Finally, the printed silver mass was determined by equations (3) and (4), using the metal's density  $\rho_{\text{Ag}} = 10.5 \text{ g cm}^{-3}$  [51].

$$V_{\text{Ag}}^{\text{IP}} = \text{Volume}_{\text{conductive tracks}} \times \emptyset_p \quad (3)$$

$$m_{\text{Ag}}^{\text{IP}} = V_{\text{Ag}}^{\text{IP}} \times \rho_{\text{Ag}} \quad (4)$$

where  $\emptyset_p$  (%),  $V_{\text{Ag}}^{\text{IP}}$  ( $\text{mm}^3$ ) and  $m_{\text{Ag}}^{\text{IP}}$  (mg) correspond to the porosity factor, volume and mass of silver determined by image processing, respectively.

##### 2.2.8.2. Topographical and geometrical analyses

Similar to the previous method, Alicona was used to determine the thickness of the lines. However, to compare the printed area with the previous method, the length and width of the lines were measured on different areas of the substrate in triplicates, using ImageJ and Alicona, respectively. Consequently, the printed volume was determined by equation (2), where the printed area is obtained by the multiplication of the line width by the length. The silver deposited mass was determined by equations (5)–(7),

$$\text{Volume}_{\text{conductive tracks}} = \text{Volume} \times \emptyset_p \quad (5)$$

$$\text{Volume}_{\text{conductive tracks}} = V_{\text{Ag}}^{\text{TOPO}} \quad (6)$$

$$m_{\text{Ag}}^{\text{TOPO}} = V_{\text{Ag}}^{\text{TOPO}} \times \rho_{\text{Ag}} \quad (7)$$

where  $V_{\text{Ag}}^{\text{TOPO}}$  ( $\text{mm}^3$ ) and  $m_{\text{Ag}}^{\text{TOPO}}$  (mg) correspond to volume and mass of deposited Ag determined by this methodology, respectively. Identically to the previous method, the porosity factor was used in the printed volume calculation.

##### 2.2.8.3. Gravimetric measurements

This methodology is based, almost exclusively, on weighting the printed samples over different steps, starting from the non-printed substrate until the ash collected after the calcination at  $900^\circ\text{C}$  of the printed substrate. All sample weights were measured in controlled atmosphere, with controlled temperature and relative humidity, to reduce the determination uncertainty.

The  $10 \times 10 \text{ cm}^2$  printed samples were weighed before and after sintering to determine the weight of the printed track, i.e. the deposited ink quantity. In parallel, the ink solid content was determined by TGA and compared with the range given by the supplier, which is quite large (between 45 to 74 wt%). With TGA, it is possible to associate the different mass losses appearing while heating the sample to the ink components, while the solid residue obtained

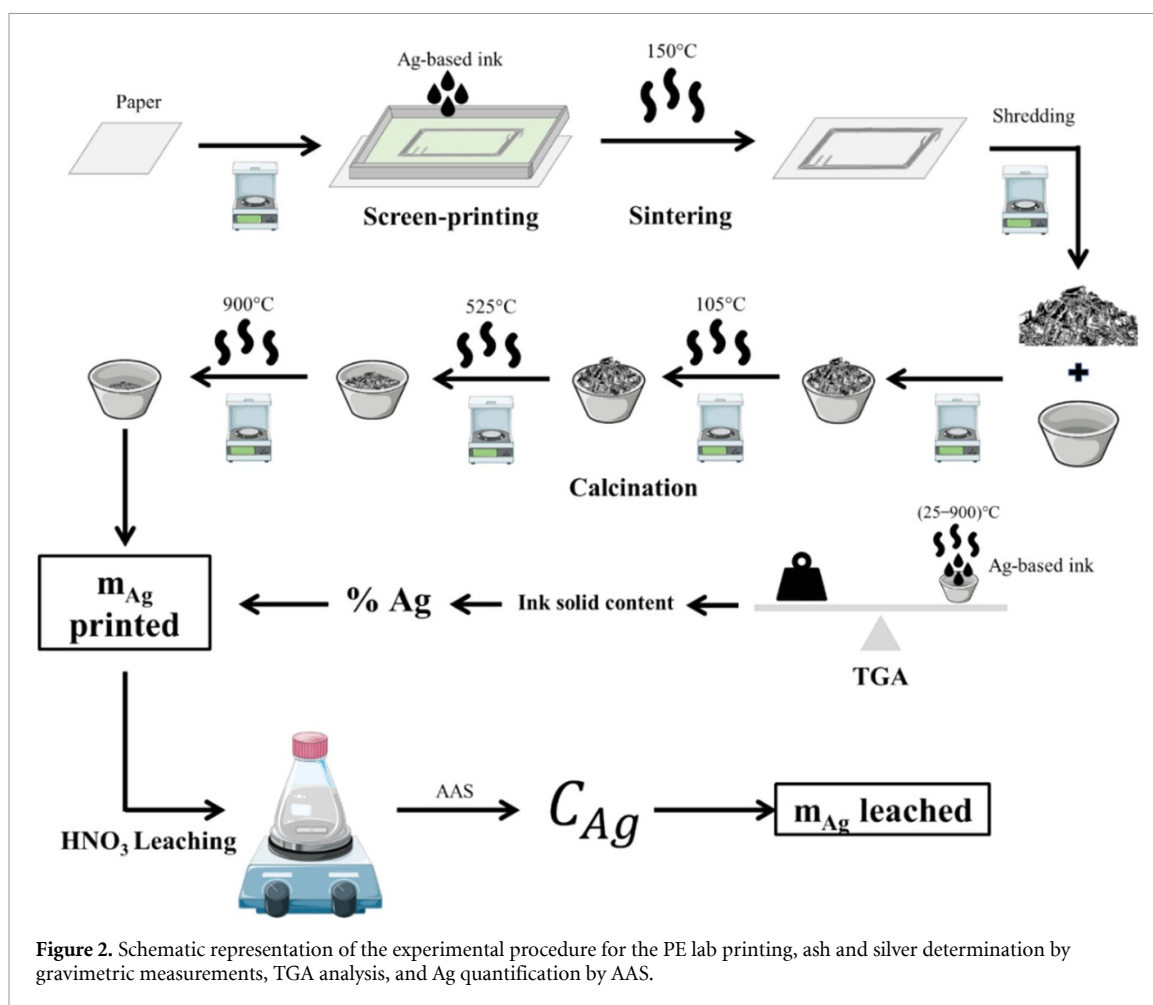


**Figure 2.** Schematic representation of the experimental procedure for the PE lab printing, ash and silver determination by gravimetric measurements, TGA analysis, and Ag quantification by AAS.

at 900 °C is considered as the ink solid content. The paper substrate and ink alone have been also studied by TGA, and classical calcinations have been performed.

The different heating steps allowed the determination of the organic content and ash fraction. In the case of the paper, ash contains only fillers whereas in the case of PE lab, Ag is also present in the ash fraction.

#### 2.2.8.4. Acid leaching and AAS quantification

This methodology consists in the lixiviation of Ag in ash and further quantification by AAS. In this work, the leaching was performed to five PE single pattern ( $10 \times 10 \text{ cm}^2$ ) ashes and five PE lab ( $30 \times 30 \text{ cm}^2$ ) ashes.

The methodology is summarized in figure 2.

### 3. Results and discussion

#### 3.1. Material elementary composition

A snapshot of a single pattern (s.p.) printed on the substrate is presented in figure 3. Aiming to better understand the material elemental composition, SEM-BSE images and respective SEM-EDS spectra were obtained for non-printed, printed samples on Powercoat™ XD80 (PE lab) and samples of the VFP-SE® ink. This qualitative technique was used to study

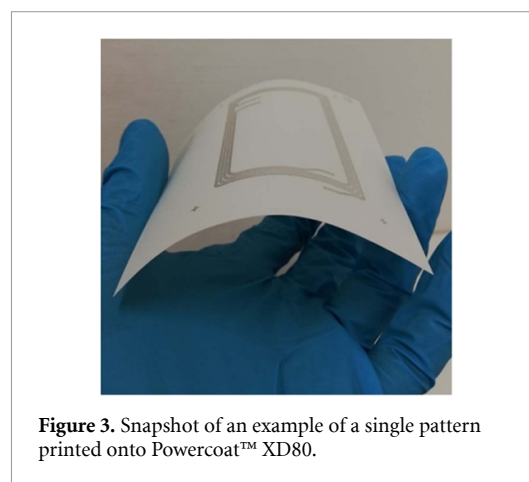


**Figure 3.** Snapshot of an example of a single pattern printed onto Powercoat™ XD80.

the structure of each cellulosic substrate, the order of magnitude of metal particles size, and the ink penetration into the substrate during printing.

Additionally, x-ray mapping was performed on the SEM-EDS images of PE lab in order to visualize the different elements spatial distribution. The cross-section SEM-EDS images, spectra, and x-ray mapping are presented in figures 4–6, respectively.

Considering all the images and spectra, different points can be outlined. Firstly, the VFP-SE® ink

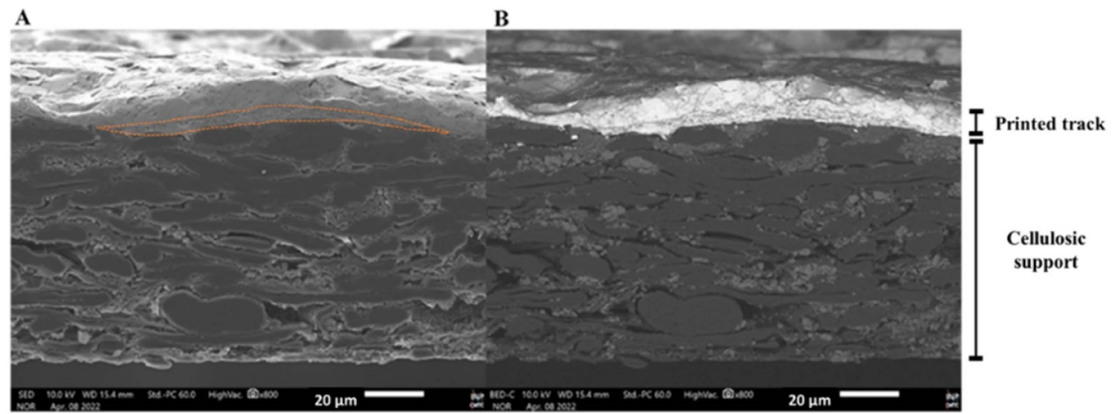


**Figure 4.** (A) PE lab SEM image. (B) PE lab SEM-BSE image. Magnification: 800x. Legend: (—) deposited ink porous region.

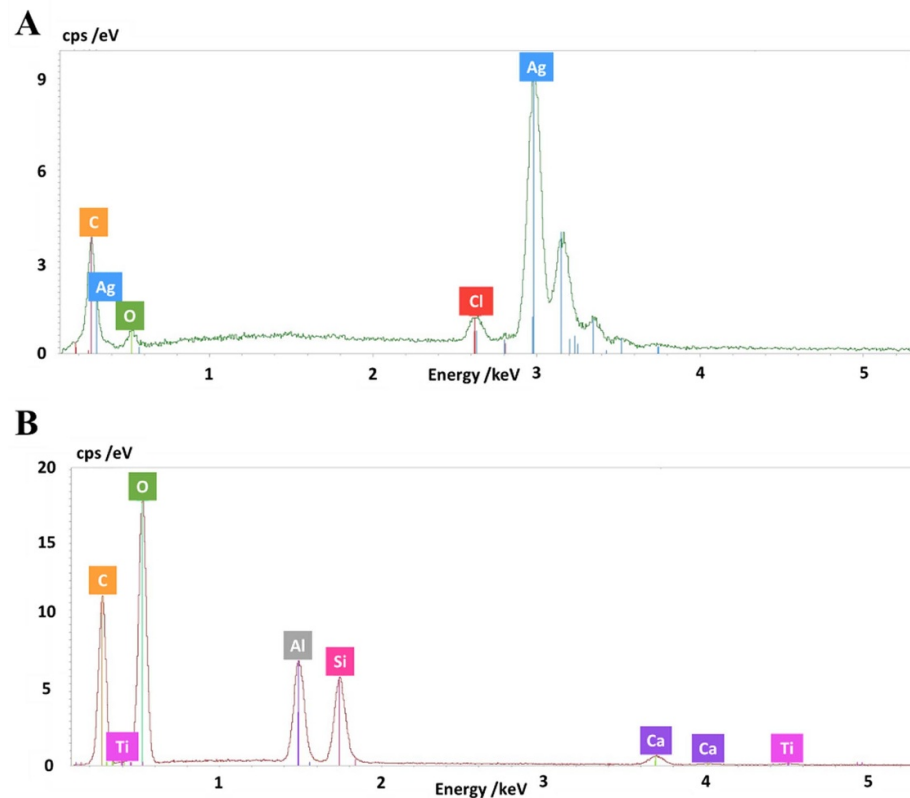


**Figure 5.** SEM-EDS spectra: (A) Ag-based ink. (B) Powercoat™ XD80 substrate.

is composed of micro-sized silver flakes with a heterogeneous distribution and is basically composed by carbon (C), oxygen (O), silver (Ag), and chlorine (Cl)—figure 5(A).

Since Powercoat™ XD80 is produced specifically for electronic applications, it presents a higher structure complexity, compared to an usual office paper [52]. SEM images confirmed that inside the fibers network the substrate is filler charged and both surfaces are coated. It was possible to detect the presence of five different elements: C, O, aluminum (Al), silicon (Si), and calcium (Ca)—figure 5(B). The presence of Ca inside of the fibers network is related to

the fillers added during the paper production process and it corresponds to  $\text{CaCO}_3$ . On the other hand, the presence of Al and Si exclusively on both surfaces of the substrate indicates the presence of a mineral pigment—kaolin—added to the coating agent. The x-ray mapping of the PE lab—figure 6—confirms the presence of both  $\text{CaCO}_3$  and kaolin in the coating layer and  $\text{CaCO}_3$  in the bulk of the cellulosic substrate. These results are in conformity with the information given by the supplier.

In the paper-making industry, the most common pigments used in coating formulations are kaolin, talc, and titanium oxide,  $\text{TiO}_2$  [53]. The presence of

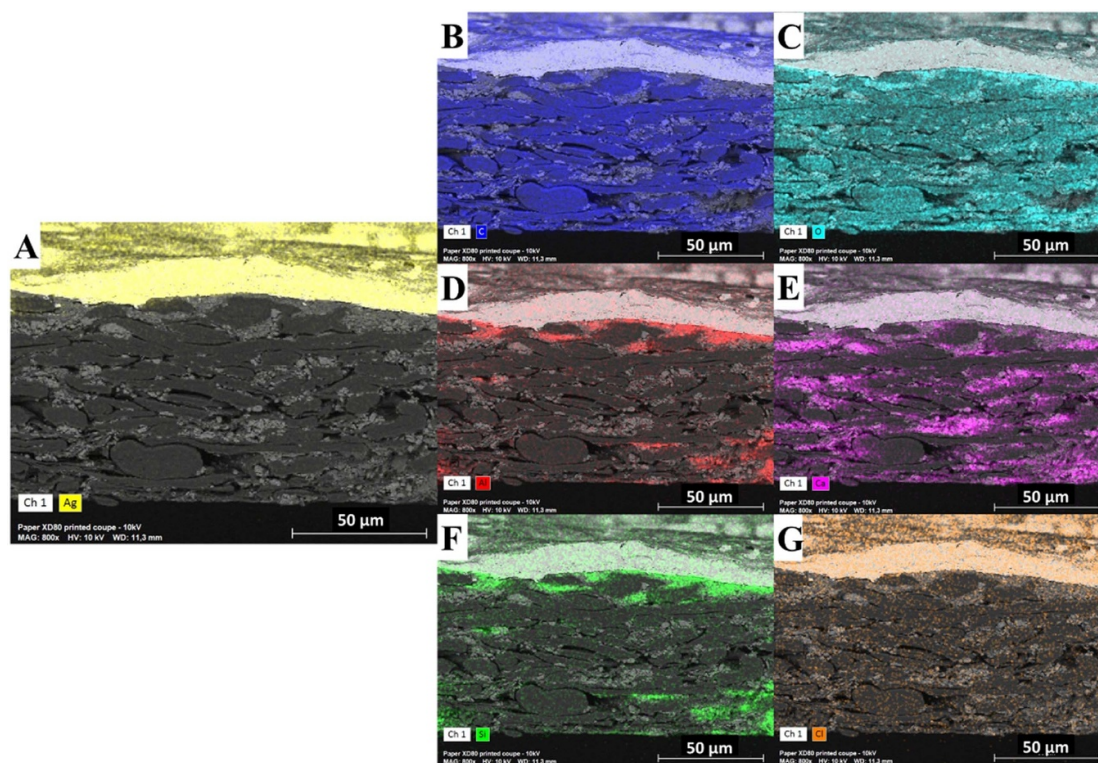


**Figure 6.** PE lab x-ray elemental mapping performed by SEM-EDS for the different chemical elements: Ag, C, O, Ca, Al, Si, and Cl (A) to (G), respectively. Magnification: 800 $\times$ .

titanium, Ti, was detected in only one of several analyzed samples with a signal close to the detection limit (1000 ppm) of the device. This may be due to its presence in the paper structure at very small concentrations or due to a contamination originating from previous productions. Similar to Ti, magnesium, Mg, was also another element detected in one sample with a signal close to the detection limit. Its presence is related with the use of magnesium silicate (talc) as one of the major fillers used in papermaking industry.

In figure 6, the x-ray mapping of the PE lab cross-section, clearly shows the layer of ink deposited on the surface of the substrate, mainly composed of silver. It is possible to outline that there is no penetration of the metallic particles into the substrate, which remain on the surface. The ink penetration is affected by both ink and substrate properties, such as viscosity, surface tension and porosity, surface energy and chemistry, respectively [54, 55].

Therefore, this feature is an important key point regarding the possible recyclability of paper-based PEs and the further separation of metal from fibers.

### 3.2. Quantification of deposited Ag onto the substrate

To develop a proper and reliable methodology to determine the amount of ink and, consequently, the amount of silver printed onto the substrate, three different strategies were investigated. To the best of our knowledge, this work is the first one that examines the

feasibility of the application of these methods for the metal quantification in PEs.

#### 3.2.1. Thresholding (image processing) and topographical analysis)

To determine the volume of the deposited ink, first, the thickness of the printed lines has been determined by Alicona. figure 7 presents the line profile of a single pattern section.

Due to the nature of the substrate it is possible to observe an irregularity of the line profile which could induce an uncertainty to the thickness measurement. Contrary to other substrates used in PE, such as plastic, ceramic, glass, etc [42], paper can be easily deformed during manufacturing of PE lab, especially after drying. Therefore, all the profiles were corrected with form removal, and the thickness was quantified. The mean thickness value of forty-eight measurements is presented in table 2.

Table 2 shows that the thickness determination using Alicona exhibited a high uncertainty ( $\pm 3.04 \mu\text{m}$ ) compared to the mean value ( $6.31 \mu\text{m}$ ). The variation coefficient reaches more than 48%. Considering the objective of determining the volume of the printed tracks, it is expected that the further results will be highly affected by the uncertainty propagation.

Figure 8 shows a section of the printed lines performed by Alicona 3D profilometer. Printing heterogeneities are visible. Consequently, it is possible to



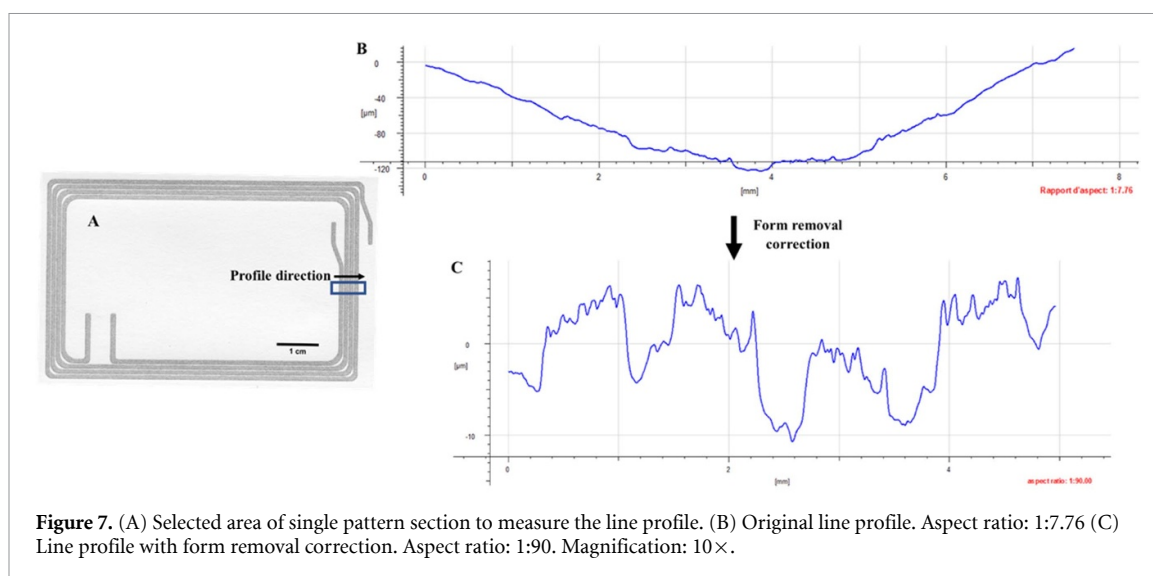


**Figure 7.** (A) Selected area of single pattern section to measure the line profile. (B) Original line profile. Aspect ratio: 1:7.76 (C) Line profile with form removal correction. Aspect ratio: 1:90. Magnification: 10 $\times$ .

**Table 2.** PE lab printed lines average thickness.

	PE lab
Thickness ( $\mu\text{m}$ )	$6.31 \pm 3.04$

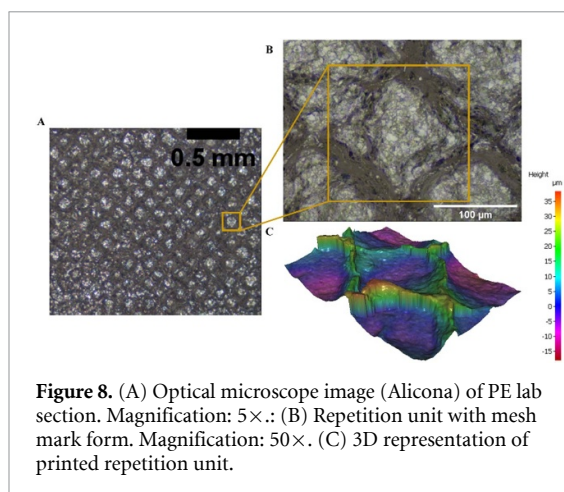


**Figure 8.** (A) Optical microscope image (Alicona) of PE lab section. Magnification: 5 $\times$ . (B) Repetition unit with mesh mark form. Magnification: 50 $\times$ . (C) 3D representation of printed repetition unit.

observe the mesh marks on the printed lines (yellow range in figure 8(B)). These marks are composed of a repetitive unit with a diamond-shape structure and is represented in Figures 8(B) and (C).

Figure 9 shows the conversion of an original image of the printed pattern on Powercoat™ XD80 into a binary image using ImageJ software. The ratio of black/white pixels allows to determine the total printed area.

Figure 9(B) presents white pixels remaining after the thresholding treatment while some false black pixels (that do not correspond to printed ink pixels) appear on the support. This can be explained by the high reflective nature of the Ag particles and, consequently, during the scanning, these regions appear white as the substrate does. Therefore, the image treatment is not able to distinguish the ink and the substrate. Additionally, the substrate is a porous

material and, during scanning, the space between the fibers contributes for the generation of black pixels, i.e. false black pixels. Optimization during thresholding is necessary to be able to obtain a printed area closer to the real value.

Figure 9(C) shows the same printed area after increasing the number of iterations to 100 and filling holes. The printed area corresponds to a mean of five different samples and is presented in table 3. Based on the dimensions of the pattern, the digital printed area is equal to 694 mm<sup>2</sup>.

Regardless of digital and thresholding printed area values (694 versus 689 mm<sup>2</sup>) being the same order, based on figure 9(B), is possible to observe that this method is not suitable because the pattern is not fully covered with black pixels. Table 3 shows a huge difference between the standard and 100 iterations thresholding printed areas (689 versus 869 mm<sup>2</sup>). Therefore, the value obtained for the 100 iterations thresholding is expected to be overestimated by this characterization. This overestimation can be related to the ink spreading.

Therefore, the printed tracks volume was determined according to equation (3), using the 100 iterations thresholding area because it provides an area value closer to a full covered black pattern. Additionally, based on the SEM-BSE cross section images (figure 4), it is possible to identify a porous region inside the deposited ink layer. Therefore, a porosity factor  $\phi_p$  of 57% was adopted [50] and included in this method to optimize the calculation of the volume of the printed patterns.

The PE single pattern (10  $\times$  10 cm<sup>2</sup>) presents a printed volume of  $3.1 \pm 1.5$  mm<sup>3</sup>, containing  $32.8 \pm 15.8$  mg of silver. Since silver volume and mass values are dependent on the thickness, high uncertainties were expected.

Therefore, it is possible to conclude that image processing was not suitable to provide a precise value of the estimated silver mass deposited onto

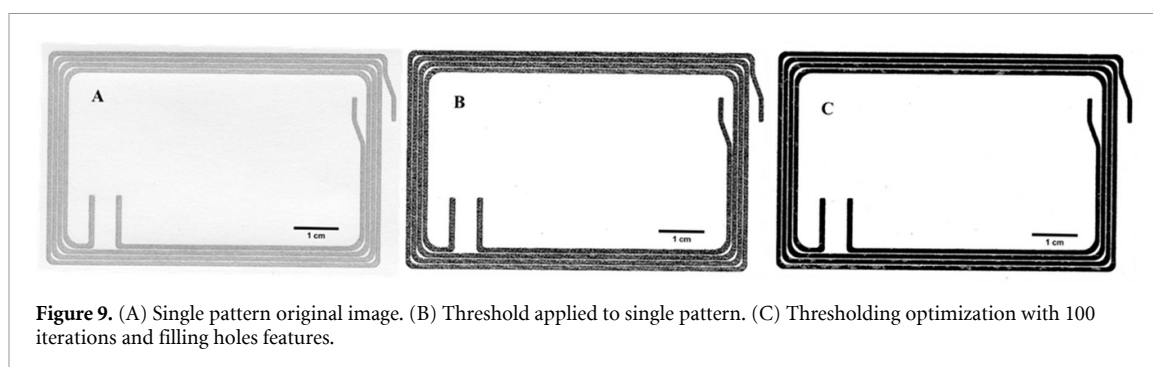
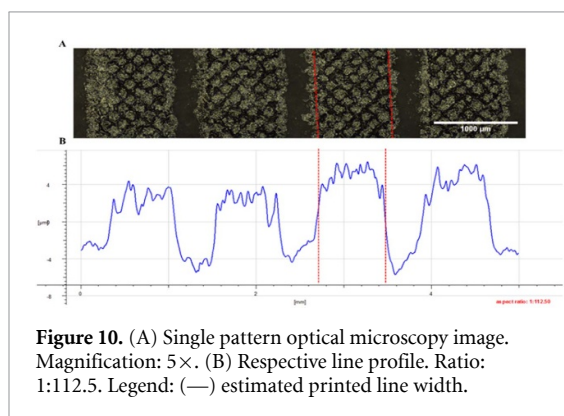


**Table 3.** Comparison of single pattern printed area using thresholding and 100 iterations thresholding.

	Thresholding	100 iterations thresholding
Printed area (mm <sup>2</sup> )	689 ± 9	869 ± 10



Powercoat™ XD80, due to both printed area overestimation and high measurement uncertainties (about 48% of the mean values).

### 3.2.2. Topographical and geometrical analyses

An alternative methodology for printed area determination by thresholding is to measure the width and length of the printed lines. This step was performed to verify the shape integrity of the printed lines and compare the printed area value with the area previously determined. Figure 10 presents a section and line profile of the printed pattern. By analyzing the lines, it is possible to observe a lateral spreading of printed ink on the substrate. This can be one of the reasons explaining why the first methodology overestimated the printed area. The spreading regions presents a lower thickness than the print itself and, therefore, the width values were measured in the region that correspond to the printed line, excluding the spreading effect.

In this method, due to the extension of the length and width measurements only one PE single pattern was analyzed. The calculation of the printed area, the ink volume, the corrected ink volume with porosity factor, and the estimation of the deposited silver mass

were made following equations (2) and (5)–(7). The volume and silver mass were determined using the thickness, the density and the  $\phi_p$  values already used in the first method.

With this second method, the printed area is  $619 \pm 3 \text{ mm}^2$ , which is closer to the theoretical one ( $694 \text{ mm}^2$ ), and lower than the printed area determined by Alicona (first method). As the calculation of the printed volume and Ag volume use the thickness, the silver mass of the PE single pattern ( $10 \times 10 \text{ cm}^2$ ),  $23.4 \pm 11.3 \text{ mg}$ , exhibits again a very high uncertainty. The second method predicts a lower silver mass compared to the first method due to the decrease of the printed area. In addition to the thickness imprecision, the hypothesis made on the selected porosity factor has a significant impact on the determination of the metal mass printed onto the substrate: higher is this value, the lower will be the Ag mass. Because of the high uncertainty on thickness, no further optimization was performed to correct the porosity factor.

Although this method is able to determine a printed area closer to the theoretical one, it is still based on geometrical measurements, i.e. the thickness, which exhibits a high uncertainty. Therefore, based on the different points previously referred, this method is neither suitable for the precise quantification of silver deposited onto paper.

### 3.2.3. Gravimetric measurements

First, TGA was performed to investigate the ink formulation alone, without any paper substrate, the objective being to determine the Ag percentage of the ink. The evolution of the ink mass over the time while heating progressively the sample in a TGA apparatus is presented in figure 11. The applied heating ramp is given in the same figure. The ink triplicates, with masses comprised between 15 and 20 mg, present a similar behavior during the test, with a solid residue at the end of experiment higher than 55 wt%. The discrepancy between the first sample and the two following ones visible in figure 11 is due to the fact that the three samples have been prepared at the same time; thus, the first sample was immediately introduced into the TGA apparatus, while the volatile chemicals of the two other samples evaporated partially before injection. This phenomenon explains the difference

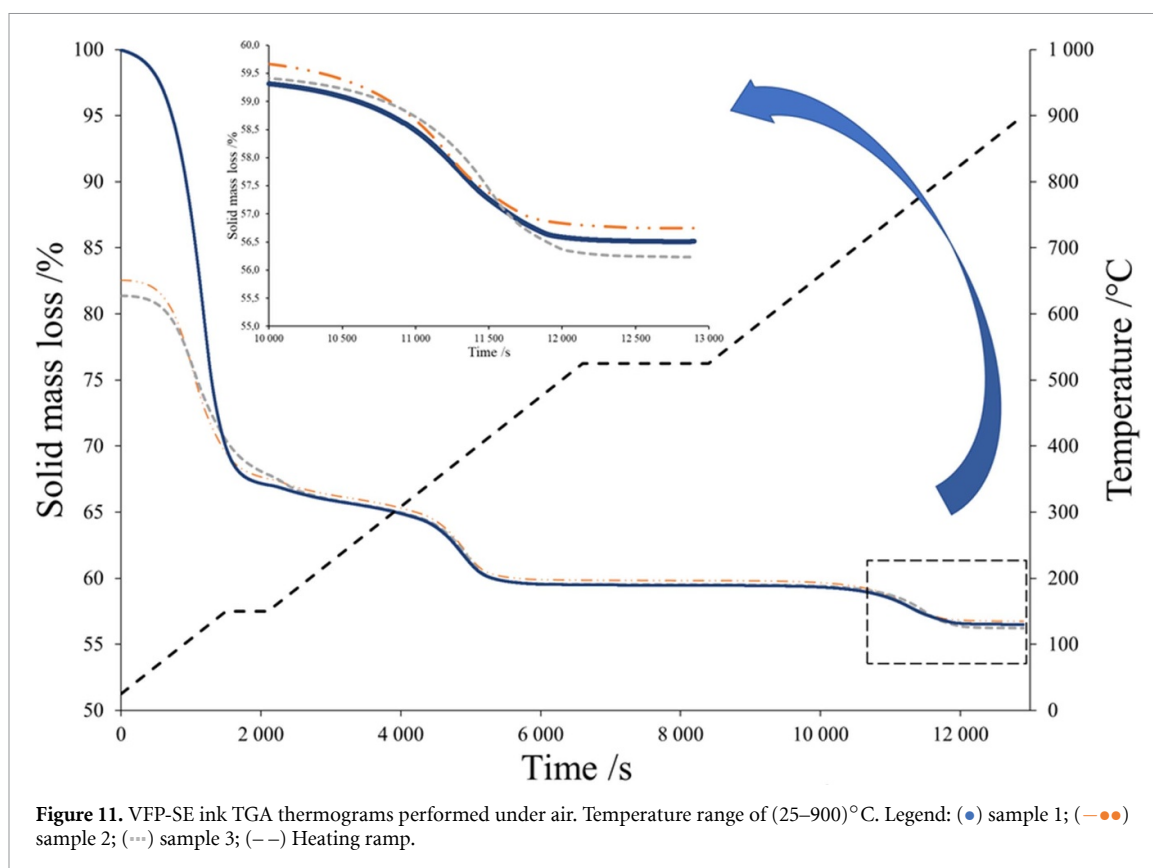


**Table 4.** VFP-SE ink solid content at 150 and 900 °C.

	VFP-SE ink
Solid content (150 °C) (wt%)	68.3 ± 0.0
Solid content (900 °C) (wt%)	56.5 ± 0.3

in the initial mass lost at temperature of approx. 25 °C. The solvent mixture, added in the ink formulation in order to make it liquid for printability, evaporated during the PE sintering, and is not any present in the final PE lab device. Except this initial difference the three obtained curves are nearly overlap.

In figure 11, it is possible to distinguish three different weight loss phenomena. Firstly, between 25 and 150 °C occurs the total evaporation of the organic solvents present in the ink formulation, corresponding approximately to 32%. Secondly, until 450 °C the ink's mass continuously decreases to a solid content of 60%. This mass loss can be related to the degradation of the binder agents. Finally, between 650 and 850 °C occurs the degradation of thermal resistant materials. After 850 °C, no further loss occurs. However, in this study, it is not possible to associate each mass loss to a specific ink constituent due to the ink formulation confidentiality and due to the fact the TGA is not coupled to mass spectrometry device. The ink formulation solid contents at 150 °C and 900 °C determined by TGA are presented in table 4.

By analyzing the solid contents, it is possible to calculate that between 150 °C and 900 °C the ink

loses 11.8% of its weight. As discussed before, this could correspond to the content of the binders inside the ink formulation after curing. Moreover, analyzing the mass loss at 900 °C in figure 10, it is possible to affirm that it remains constant until the end of the measurement, since there is no more weight loss, and the remaining mass will correspond to metallic silver, mainly, however the presence of silver oxide, Ag<sub>2</sub>O, (resulting from the silver surface oxidation) or a small proportion of silver chloride, AgCl, initially present as an impurity in the ink micro flakes, as observed in the SEM-EDS (figure 6(G)). Thus, the ink formulation contains 56.5% Ag. This is in the range given by the supplier.

In parallel the Powercoat™ XD80 was also analyzed by TGA, under the same temperature range, to assess the thermal stability of the paper substrate. The results are represented in figure 12, for an initial sample mass of 16.5 mg. For the cellulosic substrate, it is possible to identify three different degradation stages: (i) between 25 °C and 105 °C, a mass loss of 3% is observed which corresponds to water evaporation; (ii) a second mass loss of 70% is then detected between 200 °C and 525 °C, it is attributed to the degradation of different organic components present in the paper formulation, i.e. mainly hemicelluloses and cellulose, as already described by Yang *et al* [56]; (iii) finally, a third mass loss of 9% is observed from 525 °C until 900 °C, which coincides to the

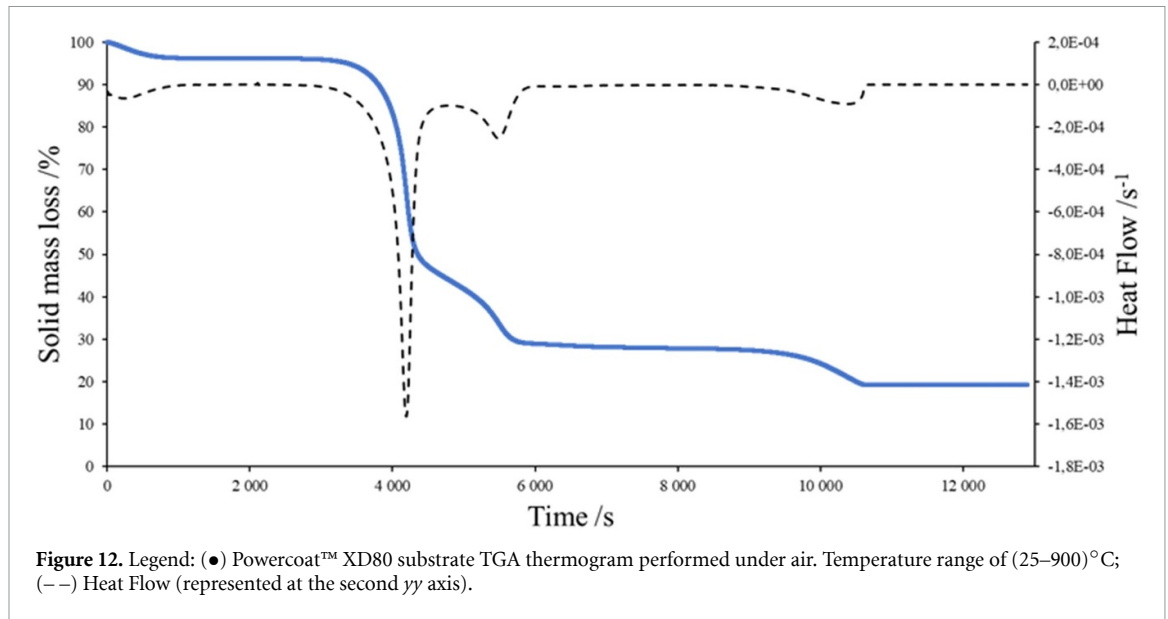
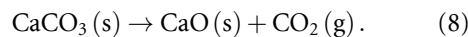


**Figure 12.** Legend: (●) Powercoat™ XD80 substrate TGA thermogram performed under air. Temperature range of (25–900) °C; (–) Heat Flow (represented at the second y axis).

**Table 5.** Powercoat™ XD80 and PE single pattern: ash and organic mass fractions based on weight measurements during calcination using  $10 \times 10 \text{ cm}^2$  samples.

	Ash cont. (%)		Organic cont. (%)
	525 °C	900 °C	
Powercoat™ XD80	$28.86 \pm 0.54$	$20.12 \pm 0.53$	$71.14 \pm 0.54$
PE s.p.	$30.09 \pm 0.28$	$21.73 \pm 1.08$	$69.91 \pm 0.28$

thermal degradation of  $\text{CaCO}_3$  filler into calcium oxide,  $\text{CaO}$ , and carbon dioxide,  $\text{CO}_2$ , as described in equations (8),



From TGA, the ash and organic contents in the Powercoat™ XD80 has been estimated at 28% and 72%. Ash is considered as the solid residue after calcination at 525 °C and the fiber content is the complement to 100%, in dry basis, i.e. excluding the mass related to water evaporation.

In parallel, the Powercoat™ XD80 and PE single pattern ( $10 \times 10 \text{ cm}^2$ ) have been also analyzed by calcination. The ash of both samples is estimated by the solid residues after calcinations at 525 °C and 900 °C and organic content is the complement to 100% at 525 °C. Results for both PE lab and Powercoat™ XD80 are summarized in table 5.

By calcination, the unprinted substrate contains 71% organic matter and 29% ash. These values are coherent since they are close to those measured by TGA on the non-printed substrate (72% and 28%, respectively). The PE lab contains 70% organic and 30% ash contents, where the difference is due to the deposited ink quantity. If ash is attributed to fillers in the Powercoat™ XD80, ash corresponds to Ag and fillers in the PE lab. This explains why ash content is slightly higher in the PE lab in comparison with the unprinted Powercoat™ XD80.

The ink content is measured after sintering (150 °C), i.e. after solvent evaporation and Ag content is considered as the residue of ink calcination at 900 °C. Finally, it was possible to retrieve the amount of silver deposited during printing, in a single pattern, as described in equations (9)–(13):

$$\% \text{ ink mass loss}_{(150-900)^\circ\text{C}} = \frac{(m_{\text{ink } 150^\circ\text{C}} - m_{\text{ink } 900^\circ\text{C}})}{m_{\text{ink } 150^\circ\text{C}}} \times 100 = 11.8 \quad (9)$$

$$m_{\text{printed ink}(150^\circ\text{C})} = m_{\text{printed XD80}(150^\circ\text{C})} - m_{\text{non-printed XD80}(150^\circ\text{C})} \quad (10)$$

$$m_{\text{printed ink}(900^\circ\text{C})} = m_{\text{printed ink}(150^\circ\text{C})} \times \left(1 - \frac{\% \text{ ink mass loss}_{(150-900)^\circ\text{C}}}{100}\right) \quad (11)$$

$$m_{\text{Ag(s.p.)}} = m_{\text{printed ink}(900^\circ\text{C})} \quad (12)$$

$$\% \text{ Ag}_{\text{s.p.}} = \frac{m_{\text{Ag(s.p.)}}}{m_{\text{pattern}(150^\circ\text{C})}} \times 100 \quad (13)$$

where  $\% \text{ ink mass loss}_{(150-900)^\circ\text{C}}$  (wt%) corresponds to the difference of ink mass between 150 °C and 900 °C. The terms  $m_{\text{printed XD80}(150^\circ\text{C})}$  (g) and  $m_{\text{non-printed XD80}(150^\circ\text{C})}$  (g) correspond to the



**Table 6.** Ag concentration and mass results of five PE single patterns and five PE lab samples using HNO<sub>3</sub> leaching.

Sample	$m_{\text{sample}}$ (g)	$m_{\text{ash leached}}$ (g)	$m_{\text{Ag}}$ (mg)
PE s.p.	$0.9216 \pm 0.0135$	$0.1926 \pm 0.0030$	$20.1 \pm 0.3$
PE lab	$7.8574 \pm 0.0162$	$1.6130 \pm 0.0039$	$137.4 \pm 4.0$

$10 \times 10 \text{ cm}^2$  sample's mass after and before printing and sintering at  $150^\circ\text{C}$ , respectively, while  $m_{\text{printed ink}}$  (g) corresponds to ink mass deposited onto the substrate after sintering at  $150^\circ\text{C}$ . The terms  $m_{\text{printed ink}}(900^\circ\text{C})$  (g) and  $m_{\text{Ag (s.p.)}}$  (g) correspond to ink mass after calcination at  $900^\circ\text{C}$  and the mass of Ag presents on each single pattern, respectively. %Ag<sub>s.p.</sub> (wt%) corresponds to the mass fraction of Ag of the device total weight.

Additionally, based on the PE single patterns weight measurement the ink content is estimated at  $2.53\% \pm 0.09\%$ . Therefore, the quantity of Ag present is  $2.23\% \pm 0.03\%$  of the sample weight. From ninety  $10 \times 10 \text{ cm}^2$  single pattern samples the average mass of before and after sintering was  $881 \pm 1 \text{ mg}$  and  $904 \pm 1 \text{ mg}$ , respectively. The difference corresponds to the ink deposited onto the substrate, an average of  $22.8 \text{ mg} \pm 1.6 \text{ mg}$ . After calcination at  $900^\circ\text{C}$ , using equation (11) the ink mass corresponds to  $88.2$  (wt%) of  $22.8 \text{ mg}$ , i.e.  $20.1 \text{ mg}$ . Therefore, the Ag mass deposited on each pattern is approximately  $20 \text{ mg}$ . Finally, Ag fraction of the first conductive layer corresponds to  $2.2 \text{ wt\%}$  of the single pattern weight.

Also, it is possible to determine the amount of Ag present in the ash of a single pattern, as described in equations (14) and (15):

$$m_{\text{ash}} = m_{\text{s.p.}} \times \text{Ash cont.}_{900^\circ\text{C}} \quad (14)$$

$$\% \text{Ag/Ash}_{\text{s.p.}} = \frac{m_{\text{Ag (s.p.)}}}{m_{\text{ash}}} \times 100 \quad (15)$$

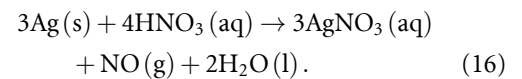
where,  $\text{Ash cont.}_{900^\circ\text{C}}$  (wt%) corresponds to ash weight fraction of the single pattern after calcination at  $900^\circ\text{C}$ . The terms  $m_{\text{ash}}$  (g) and %Ag/Ash<sub>s.p.</sub> (wt%) correspond to the single pattern mass ratio of Ag in the ash. Considering the ash content at  $900^\circ\text{C}$ , previously presented in table 5, the %Ag/Ash determined by equation (15) is equal to  $10.1 \text{ wt\%}$ .

After the characterization and quantification of Ag on single printed patterns, it was possible to estimate the Ag quantity for PE lab samples. Please keep in mind that in this case the  $30 \times 30 \text{ cm}^2$  samples were printed with 6 patterns, as represented in figure 1. Hence, each PE lab sheet should contain  $120 \text{ mg}$  of Ag. Based on the substrate basis weight, each non-printed sheet weights approximately  $7.74 \pm 0.36 \text{ g}$ . Therefore, Ag fraction correspond to  $1.5 \text{ wt\%}$  of PE lab weight. After calcination at  $900^\circ\text{C}$  of five different PE lab samples, the obtained ash weighted  $1.64 \text{ g}$

corresponding to an ash content of  $21.2 \text{ wt\%}$ . Finally, the %Ag/Ash is estimated to be  $7.3 \text{ wt\%}$ .

### 3.2.4. Acid leaching and AAS analysis

Inspire by hydrometallurgy, acid leaching can be used to dissolve the metals present in the ash. In this study, HNO<sub>3</sub> was used as a leaching agent, that has both the capacity to dissolve silver and is less toxic compared to other leaching reagents, such as cyanide [57, 58]. The simplified dissolution reaction of silver by HNO<sub>3</sub> is described by equation (16) [59]. The average Ag concentration and mass of both samples are presented in table 6,



By the analysis of table 6, it is possible to conclude that PE single pattern presents a silver mass identical to the value determined by the previous method, with an average of  $20.1 \pm 0.3 \text{ mg}$  of Ag. Furthermore,  $10.5 \pm 0.3\%$  of the leached ash is composed of Ag, and  $2.2\%$  of the pattern weight corresponds to Ag. Regarding the PE lab leaching, the results presented a slightly higher amount of metal, with  $137 \text{ mg}$  of Ag, corresponding to a %Ag/Ash of  $8.5 \pm 0.1\%$ . The multi pattern sample is composed by  $1.7\%$  of Ag.

To summarize, the Ag masses printed onto the single pattern determined by the four different methodologies are presented in table 7.

By the analysis of table 7 it is possible to observe the disparity of Ag mass values between the assessed methods. Due to the overestimation of the printed area based on image processing, this methodology corresponds to the highest Ag mass printed onto the sample,  $33 \text{ mg}$  per sample. The measurement of the printed tracks length and width, by the second methodology, decreases the printed area value and, consequently, reduces Ag mass to  $23 \text{ mg}$  per sample. However, both methods suffer from a lack of precision since the dispersion is half of the mean value. The methodology based on gravimetric measurements gave a lower Ag mass,  $20.3 \text{ mg}$  per sample. In addition, this method is more accurate than both first and second methods, as it presents results with the lowest dispersion of  $7\%$ , instead of  $48\%$ . A disadvantage that can be associated with the third methodology is the need to performing TGA analysis on each ink to determine the %ink mass loss<sub>(150–900)°C</sub> because this parameter is dependent on the ink formulation.

**Table 7.** Comparison of printed silver mass on a single pattern determined by the four different methods.

	Methods			
	a.	b.	c.	d.
Ag mass (mg)	$32.8 \pm 15.8$	$23.4 \pm 11.3$	$20.3 \pm 1.4$	$20.1 \pm 0.3$

Legend: a—thresholding; b—topographical and geometrical method; c—gravimetric method; d—HNO<sub>3</sub> leaching.

Finally, comparing the Ag mass determined by all methods, the leaching method is direct, simpler to perform and provides a more accurate Ag mass value of 20.1 mg. Despite the fact that calcination is a destructive method, it presents the advantage of using less approximations and be independent of the print dimensions, i.e. it does not include additional factors and, consequently, no additional experimental uncertainties.

#### 4. Conclusions and perspectives

Four different methodologies were evaluated for the quantification of Ag printed onto paper during the manufacturing of PEs. Thresholding demonstrated an overestimation of the printed area and, consequently, an excess of Ag deposited. This was attributed mainly to the mismatch of the thresholding applied to metallic ink, caused by the ink spreading on the substrate surface. The determination of printed area by measuring printed lines width and length was evaluated in the second method. Due to the nature of the substrate, the thickness measurement by topographical analysis is inaccurate, resulting in high measurements uncertainties for both methods. The quantification of Ag by gravimetric measurements was performed in the third method. Finally, the method which is based on HNO<sub>3</sub> leaching presented more accurate results. This method determined that the studied single pattern ( $10 \times 10 \text{ cm}^2$ ) has 20.1 mg of Ag, corresponding to 2.2% of the pattern weight, while PE lab is composed by 1.7% of Ag, equivalent to 137 mg.

Considering devices of a high added-value, a non-destructive method should be preferred to quantify the silver amount to be tracked. Nevertheless, in the present article, non-destructive methods showed several drawbacks failing thus to give reliable results. Therefore, the destructive method, based on PE sample calcination and HNO<sub>3</sub> leaching followed by AAS determinations gave more accurate results and should be employed preferably.

Nowadays, the emerging PE industry, which mainly uses metal-based inks will require simple methods to quantify and assess the circularity of the added-value materials used. Therefore, with the purpose of recycling, it is of primary importance to develop a rigorous method to quantify the amount

of silver initially loaded and track it all along the recycling steps. The impact on environment should therefore be evaluated.

#### Data availability statement

The data cannot be made publicly available upon publication because they are not available in a format that is sufficiently accessible or reusable by other researchers. The data that support the findings of this study are available upon reasonable request from the authors.

#### Acknowledgments

Authors would like to thank to Fedrigoni in the person of G Déprès for providing the Powercoat™ XD80 paper and the RFID antenna pattern, and B Khelifi and F Roussel for performing SEM-EDS analysis. Additionally, we want to thank the Grenoble INP-Phelma school for the access and utilization of the AAS equipment.

This work is supported by the Agence Nationale de la Recherche (French National Research Agency) in the framework of the ‘Investissements d’avenir’ program (ANR-15-IDEX-02), within the project SAVE. LGP2 is part of the LabEx Tec 21 (Investissements d’Avenir—grant agreement n° ANR-11-LABX-0030) and of PolyNat Carnot Institute (Investissements d’Avenir—Grant Agreement n° ANR-16-CARN-0025-01). This research was made possible thanks to the facilities of the TekLiCell platform funded by the Région Rhône-Alpes (ERDF: European Regional Development Fund).

#### CRedit authorship contribution statement

João H F Conceição: Investigation, Visualization, Writing—original draft.

M Party: Investigation.

D Curtil: Investigation, Visualization, Conceptualization.

L Švecová: Conceptualization, Supervision, Writing—review & editing.

N Marlin: Conceptualization, Supervision, Writing—review & editing.

N Reverdy-Bruas: Conceptualization, Supervision, Writing—review & editing.

## Conflict of interest

The authors declare that they have no known competing financial interests or personal relationships that could have appeared to influence the work reported in this paper.

## ORCID iDs

João H F Conceição  <https://orcid.org/0000-0002-6641-6194>

D Curtil  <https://orcid.org/0000-0001-8264-0308>

L Švecová  <https://orcid.org/0000-0003-2439-2646>

N Marlin  <https://orcid.org/0000-0003-2248-6104>

N Reverdy-Bruas  <https://orcid.org/0000-0001-5302-3749>

## References

- [1] Wiklund J, Karakoç A, Palko T, Yigitler H, Ruttik K, Jäntti R and Paltakari J 2021 A review on printed electronics: fabrication methods, inks, substrates, applications and environmental impacts *J. Manuf. Mater. Process.* **5** 1–36
- [2] Glogic E, Futsch R, Thenot V, Iglesias A, Joyard-Pitiot B, Depres G, Rougier A and Sonnemann G 2021 Development of eco-efficient smart electronics for anticounterfeiting and shock detection based on printable inks *ACS Sustain. Chem. Eng.* **9** 11691–704
- [3] Martins R, Gaspar D, Mendes M J, Pereira L, Martins J, Bahubalindruni P, Barquinha P and Fortunato E 2018 Papertronics: multigate paper transistor for multifunction applications *Appl. Mater. Today* **12** 402–14
- [4] Nandy S et al 2021 Cellulose: a contribution for the zero e-waste challenge *Adv. Mater. Technol.* **6** 2000994
- [5] Tobjörk D and Österbacka R 2011 Paper electronics *Adv. Mater.* **23** 1935–61
- [6] Research P 2021 *Printed Electronics Market Size to Hit USD 44.4 Bn by 2030*
- [7] Wu W 2017 Inorganic nanomaterials for printed electronics: a review *Nanoscale* **9** 7342–72
- [8] Hu G, Kang J, Ng I W T, Zhu X, Howe R C T, Jones C G, Hersam M C and Hasan T 2018 Functional inks and printing of two-dimensional materials *Chem. Soc. Rev.* **47** 3265–300
- [9] Blayo A 2017 Printing ink formulation *Printing Inks—Grenoble INP Pagora lecture book* pp 1–19
- [10] Kantola V, Kulovesi J, Lahti L, Lin R, Zavodchikova M and Coatanéa E 2009 Printed electronics, now and future *Bit Bang—Rays to the Future* pp 63–102
- [11] Machiels J, Verma A, Appeltans R, Buntinx M, Ferraris E and Deferme W 2020 Printed electronics (PE) as an enabling technology to realize flexible mass customized smart applications *Proc. CIRP* **96** 115–20
- [12] Lin Y, Gritsenko D, Liu Q, Lu X and Xu J 2016 Recent advancements in functionalized paper-based electronics *ACS Appl. Mater. Interfaces* **8** 20501–15
- [13] Sani N, Wang X, Granberg H, Andersson Ersman P, Crispin X, Dyreklev P, Engquist I, Gustafsson G and Berggren M 2016 Flexible lamination-fabricated ultra-high frequency diodes based on self-supporting semiconducting composite film of silicon micro-particles and nano-fibrillated cellulose *Sci. Rep.* **6** 1–8
- [14] Damnali O F and Eskizeybek V 2019 Synergistic impact of graphene and carbon nanotubes on waste paper for hybrid nanocomposite substrates *Cellulose* **26** 3935–54
- [15] Martins R, Nathan A, Barros R, Pereira L, Barquinha P, Correia N, Costa R, Ahnood A, Ferreira I and Fortunato E 2011 Complementary metal oxide semiconductor technology with and on paper *Adv. Mater.* **23** 4491–6
- [16] Carvalho J T, Dubceac V, Grey P, Cunha I, Fortunato E, Martins R, Clausner A, Zschech E and Pereira L 2019 Fully printed zinc oxide electrolyte-gated transistors on paper *Nanomaterials* **9** 1–9
- [17] Huang J 1995 Microstrip antennas for commercial applications *Microstrip Antennas—The Analysis and Design of Microstrip Antennas and Arrays* ed D M Pozar and D H Schaubert (Wiley) pp 371–9
- [18] Garg R, Bhartia P, Bahl I and Ittipiboon A 2001 Microstrip radiators *Microstrip Antenna Design Handbook* ed R Garg, P Bhartia, I Bahl and A Ittipiboon (Artech House, Inc.) pp 54–72
- [19] Down M P, Foster C W, Ji X and Banks C E 2016 Pencil drawn paper based supercapacitors *RSC Adv.* **6** 81130–41
- [20] Yao B, Yuan L, Xiao X, Zhang J, Qi Y, Zhou J, Zhou J, Hu B and Chen W 2013 Paper-based solid-state supercapacitors with pencil-drawing graphite/polyaniline networks hybrid electrodes *Nano Energy* **2** 1071–8
- [21] Ferreira I, Brás B, Martins J I, Correia N, Barquinha P, Fortunato E and Martins R 2011 Solid-state paper batteries for controlling paper transistors *Electrochim. Acta* **56** 1099–105
- [22] Avoundjian A, Galvan V and Gomez F A 2017 An inexpensive paper-based aluminum-air battery *Micromachines* **8** 1–11
- [23] Mohammadifar M and Choi S 2017 A papertronic, on-demand and disposable biobattery: saliva-activated electricity generation from lyophilized exoelectrogens preinoculated on paper *Adv. Mater. Technol.* **2** 1–9
- [24] Zhou Y, Fuentes-Hernandez C, Khan T M, Liu J C, Hsu J, Shim J W, Dindar A, Youngblood J P, Moon R J and Kippelen B 2013 Recyclable organic solar cells on cellulose nanocrystal substrates *Sci. Rep.* **3** 24–26
- [25] Leonat L, White M S, Glowacki E D, Scharber M C, Zillger T, Rühling J, Hübner A and Sariciftci N S 2014 4% efficient polymer solar cells on paper substrates *J. Phys. Chem. C* **118** 16813–7
- [26] Rawat M, Jayaraman E, Balasubramanian S and Iyer S S K 2019 Organic solar cells on paper substrates *Adv. Mater. Technol.* **4** 1–11
- [27] Cinti S, Cinotti G, Parolo C, Nguyen E P, Caratelli V, Moscone D, Arduini F and Merkoci A 2020 Experimental comparison in sensing breast cancer mutations by signal on and signal off paper-based electroanalytical strips *Anal. Chem.* **92** 1674–9
- [28] Khaliliazar S, Toldrà A, Chondrogiannis G and Hamed M M 2021 Electroanalytical paper-based nucleic acid amplification biosensors with integrated thread electrodes *Anal. Chem.* **93** 14187–95
- [29] Merilampi S, Ukkonen L, Sydänheimo L, Ruuskanen P and Kivikoski M 2007 Analysis of silver ink bow-tie RFID tag antennas printed on paper substrates *Int. J. Antennas Propag.* **2007** 1–9
- [30] Çiftçi T, Karaosmanoğlu B and Ergül Ö 2016 Low-cost inkjet antennas for RFID applications *IOP Conf. Ser.: Mater. Sci. Eng.* **120** 1–2
- [31] Abutarboush H F and Shamim A 2012 Paper-based inkjet-printed tri-band u-slot monopole antenna for wireless applications *IEEE Antennas Wirel. Propag. Lett.* **11** 1234–7
- [32] Kim S, Kawahara Y, Georgiadis A, Collado A and Tentzeris M M 2013 Low-cost inkjet-printed fully passive RFID tags using metamaterial-inspired antennas for capacitive sensing applications *IEEE MTT-S Int. Microw. Symp. Dig* pp 3–6
- [33] Nair R, Barahona M, Betancourt D, Schmidt G, Bellmann M, Hoft D, Plettemeier D, Hubler A and Ellinger F 2014 A fully printed passive chipless RFID tag for low-cost mass production *8th Eur. Conf. Antennas Propagation, EuCAP 2014* pp 2950–4

- [34] Aliaga C, Zhang H, Dobon A, Hortal M and Beneventi D 2015 The influence of printed electronics on the recyclability of paper: a case study for smart envelopes in courier and postal services *Waste Manage.* **38** 41–48
- [35] Sundriyal P and Bhattacharya S 2017 Inkjet-printed electrodes on A4 paper substrates for low-cost, disposable, and flexible asymmetric supercapacitors *ACS Appl. Mater. Interfaces* **9** 38507–21
- [36] De Araujo W R and Paixão W R 2014 Fabrication of disposable electrochemical devices using silver ink and office paper *Analyst* **139** 2742–7
- [37] Cenci M P, Scarazzato T, Munchen D D, Dartora P C, Veit H M, Bernardes A M and Dias P R 2021 Eco-friendly electronics—a comprehensive review *Adv. Mater. Technol.* **7** 1–34
- [38] Hu J and Ismail M 2011 Green electronics CMOS *High Efficiency On-chip Power Management* pp 3–14
- [39] Andrae A, Xia M, Zhang J and Tang X 2016 Practical eco-design and eco-innovation of consumer electronics—the case of mobile phones *Challenges* **7** 3–21
- [40] European Commission 2008 *Waste Framework Directive 2008/98/EC*
- [41] Starešinić M, Muck T, Stanić M and Gunde M K 2011 Development of image analysis procedures for evaluation of printed electronics quality *Inf. MIDEA* **41** 12–17
- [42] Faddoul R, Reverdy-Bruas N, Blayo A, Haas T and Zeilmann C 2012 Optimisation of silver paste for flexography printing on LTCC substrate *Microelectron. Reliab.* **52** 1483–91
- [43] Czajkowski J, Prykäri T, Alarousu E, Palosaari J and Myllylä R 2010 Optical coherence tomography as a method of quality inspection for printed electronics products *Opt. Rev.* **17** 257–62
- [44] VFP ink technologies VFP silver electron (SE) *Tech. Data Sheet*
- [45] Arjowiggins 2005 Technical data sheet powercoat *Tech. Data Sheet*
- [46] Standard I 2008 ISO 638–2008
- [47] TAPPI T 211 om-12 2002 Ash in wood, pulp, paper and paperboard: combustion at 525 °C *TAPPI Test Methods* (Tech. Assoc. Pulp and Pap. Ind. Atlanta, GA. Tappi Press) pp 1–5
- [48] TAPPI T 413 om-11 2002 Ash in wood, pulp, paper and paperboard: combustion at 900 °C *TAPPI Test Methods* (Tech. Assoc. Pulp and Pap. Ind. Atlanta, GA. Tappi Press) pp 1–5
- [49] Anon 2013 TAPPI T 402 sp-13: standard conditioning and testing atmospheres for paper, board, pulp handsheets, and related products
- [50] Thenot V 2017 *Impression et recuits sélectifs d'encre métalliques sur papier—Optimisation des propriétés électriques de boucles RFID-HF en vue d'une production industrielle* (University Grenoble Alpes)
- [51] Haynes W M, Lide D R and Bruno T J 2017 Physical constants of inorganic compounds *CRC Handbook of Chemistry and Physics* 97th edn (Taylor and Francis Group, LLC) pp 4.85–6
- [52] Vicente A T, Araujo A, Gaspar D, Santos L, Marques A, Mendes M J, Pereira L, Fortunato E and Martins R 2017 Optoelectronics and bio devices on paper powered by solar cells *Nanostructured Solar Cells* pp 34–65
- [53] Belgacem M N and Bras J 2016 Surface treatments of paper *Lignocellulosic Fibers and Wood Handbook: Renewable Materials for Today's Environment* ed M N Belgacem and A Pizzi (Wiley-VCH) pp 481–92
- [54] Krainer S, Smit C and Hirn U 2019 The effect of viscosity and surface tension on inkjet printed picoliter dots *RSC Adv.* **9** 31708–19
- [55] Jansson E, Lyytikäinen J, Tanninen P, Eiroma K, Leminen V, Immonen K and Hakola L 2022 Suitability of paper-based substrates for printed electronics *Materials* **15** 957–74
- [56] Yang H, Yan R, Chen H, Lee D H and Zheng C 2007 Characteristics of hemicellulose, cellulose and lignin pyrolysis *Fuel* **86** 1781–8
- [57] Birich A, Friedrich B and Wotruba H 2018 Alternative silver production by environmental sound processing of a sulfo salt silver mineral found in Bolivia *Metals* **8** 114–34
- [58] Holloway P C, Merriam K P and Etsell T H 2004 Nitric acid leaching of silver sulphide precipitates *Hydrometallurgy* **74** 213–20
- [59] Martínez L L, Segarra M, Fernández M and Espiell F 1993 Kinetics of the dissolution of pure silver and silver-gold alloys in nitric acid solution *Metall. Trans. B* **24** 827–37